

Continual Learning with Vision-Language Models via Semantic-Geometry Preservation

Chiyan He, Zihuan Qiu, Fanman Meng, *Member, IEEE*, Runtong Zhang, Linfeng Xu, *Member, IEEE*, Qingbo Wu, *Member, IEEE*, Hongliang Li, *Senior Member, IEEE*

Abstract—Continual learning of pretrained vision-language models (VLMs) is prone to catastrophic forgetting, yet current approaches adapt to new tasks without explicitly preserving the cross-modal semantic geometry inherited from pretraining and previous stages, allowing new-task supervision to induce geometric distortion. We observe that the most pronounced drift tends to concentrate in vulnerable neighborhoods near the old-new semantic interface, where shared visual patterns are easily re-explained by new textual semantics. To address this under an exemplar-free constraint, we propose Semantic Geometry Preservation for Continual Learning (SeGP-CL). SeGP-CL first probes the drift-prone region by constructing a compact set of adversarial anchors with dual-targeted projected gradient descent (DPGD), which drives selected new-task seeds toward old-class semantics while remaining faithful in raw visual space. During training, we preserve cross-modal structure by anchor-guided cross-modal geometry distillation (ACGD), and stabilize the textual reference frame across tasks via a lightweight text semantic-geometry regularization (TSGR). After training, we estimate anchor-induced raw-space drift to transfer old visual prototypes and perform dual-path inference by fusing cross-modal and visual cues. Extensive experiments on five continual learning benchmarks demonstrate that SeGP-CL consistently improves stability and forward transfer, achieving state-of-the-art performance while better preserving semantic geometry of VLMs.

Index Terms—Continual learning, vision-language model, semantic geometry, knowledge distillation

I. INTRODUCTION

CONTINUAL learning (CL) aims to enable deep models to accumulate knowledge from a stream of tasks while mitigating catastrophic forgetting of previously acquired capabilities. With the emergence of large-scale pretrained vision-language models (VLMs) such as CLIP [1] and ALIGN [2], the CL paradigm is undergoing a notable shift: empowered by strong cross-modal representation alignment, VLMs can leverage stable and semantically explicit textual concepts to organize ever-growing downstream visual data, making them particularly suitable for class-incremental continual learning [3], [4] and related settings [5], [6], [7]. Despite this promise, CL upon pretrained VLMs remains highly challenging. Early studies often adopt conservative strategies by attaching task-specific or class-specific components to an otherwise frozen VLM backbone [8], [9], [10], [3]. These methods implicitly treat inter-task knowledge as primarily interfering, favoring

Corresponding author: Fanman Meng. The authors are with the School of Information and Communication Engineering, University of Electronic Science and Technology of China, Chengdu 611731, China (e-mail: {cyhe;zihuanqiu;rtzhang}@std.uestc.edu.cn; {fmmeng;lfxu;qbwu;hlli}@uestc.edu.cn).

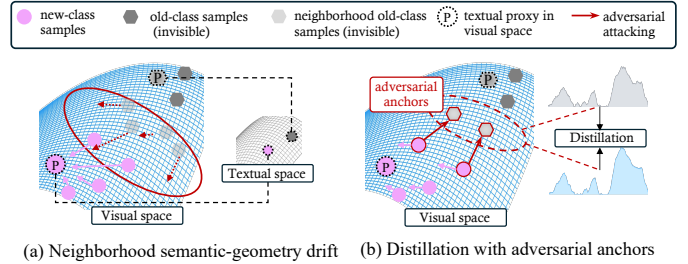


Fig. 1. Boundary vulnerability in VLM-based continual learning and our remedy. (a) Shared visual patterns near the old-new semantic interface are re-explained by new-task texts, leading to cross-modal semantic-geometry distortion and forgetting. (b) We construct adversarial anchors toward old-class semantics and perform anchor-guided cross-modal geometry distillation (ACGD) to constrain the drift in this vulnerable region.

isolation over transfer. However, such an assumption does not fully align with the general-purpose cross-modal structure learned by VLM pretraining. More recent efforts have shown progress by directly updating the VLM itself through parameter-efficient or structured adaptation schemes [11], [12], [13]. Nevertheless, these approaches are largely general continual adaptation techniques and lack targeted modeling of cross-modal stability and knowledge transfer mechanisms. Another line of work begins to explicitly exploit the cross-modal priors of VLMs. In particular, these works exploit the rich representational capacity of the text modality (e.g., attributes, concepts, and semantic hierarchies) to facilitate anti-forgetting continual learning [14], [15], [16]. Yet, these methods still provide limited attention to *preserving the established cross-modal geometry under the exemplar-free constraint*.

Recent studies have observed that abrupt representation variation induced by incremental updates can impair the cross-modal geometry of VLMs [17], [18], [19]. However, existing solutions are often conservative (e.g., early stopping or regularization with reference data [20], [21]), and they struggle to precisely constrain the regions that are most susceptible to geometry distortion. Our key observation is that when a VLM is adapted with new-task supervision, harmful drift does not occur uniformly in the embedding space. Instead, it tends to concentrate around the old-new semantic interface, where incoming samples share visual patterns with previously learned concepts and these shared visual patterns are therefore prone to being re-explained by newly introduced textual semantics. As illustrated in Fig. 1(a), during new-task learning, once these shared patterns are pulled toward new semantics, the established visual-text alignment inherited from old tasks can

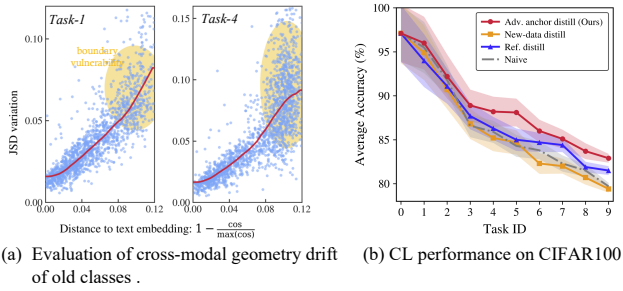


Fig. 2. Empirical evidence of boundary vulnerability and comparison of distillation schemes. (a) We measure the distributional shift in cross-modal semantics with Jensen-Shannon divergence (JSD) [22]; markedly larger drift is observed around the semantic interface (visual feature has a low similarity with its corresponding text embedding) after an incremental-task update. (b) We compare cross-modal distillation using different data sources: new-task data, reference data [20], [19], and our adversarial anchors.

be disrupted and lead to pronounced forgetting. To quantify how severely the established cross-modal geometry is perturbed, we measure the cross-modal distributional shift after an incremental-task update as a proxy of geometric distortion, using the Jensen-Shannon divergence (JSD) [22] between the pre- and post-update similarity distributions. Fig. 2(a) shows a markedly amplified shift near the semantic interface, indicating that cross-modal geometry distortion is primarily triggered by boundary neighborhoods rather than the core regions of old semantics. Therefore, the key is to *protect these vulnerable regions of cross-modal geometry, especially without old data*.

Inspired by findings on the adversarial robustness of VLMs [23], [24], [25], we leverage a practical insight: if tiny, targeted perturbations can quickly alter image-text relations, then such perturbations can be used constructively to expose and cover the most vulnerable neighborhoods of the old geometry. This motivates our design under the exemplar-free constraint: rather than synthesizing images that merely “look like old classes” [26], [27], [28], we propose to construct a small set of adversarial anchors that ‘push’ new samples into old-class decision regions, thereby concentrating constraints on the boundary neighborhoods where updates are most prone to distort the established cross-modal geometry (Fig. 1(b)).

To construct anchors, we propose Dual-targeted Projected Gradient Descent (DPGD), which pushes a new-task seed toward a selected old-class text embedding while constraining it to remain close to the corresponding visual prototype. The visual target compensates for the modality gap [29] and prevents purely text-targeted attacks from generating unstable or visually irrelevant anchors. As a result, the anchors concentrate on the vulnerable old-semantics neighborhoods close to the new-task semantics. We then apply Anchor-guided Cross-modal Geometry Distillation (ACGD) on these anchors to efficiently probe the drift-prone region and preserve the learned structure. Fig. 2(b) shows that, compared to the baseline of naive finetune with Low-Rank Adaptation (LoRA) [30], anchor-guided distillation is significantly more favorable to CL task, whereas distilling old-class signals directly on raw new-task samples performs the worst; distillation with reference data [19] provides a strong general constraint but is less targeted to the drift-prone regions.

In addition, we introduce a Text Semantic Geometry Regularization (TSGR) to stabilize the textual semantic “reference frame” during continual updates. The reliability of cross-modal alignment depends not only on the visual-text relations at the trigger-region anchors, but also on the relative geometric structure among textual concepts (e.g., neighborhood relations and semantic hierarchies). If this structure is distorted across tasks, the semantic coordinates of old classes can be implicitly re-parameterized, causing old knowledge to degrade even when local distillation constraints are satisfied. TSGR constrains concept-wise relative relations through a key relational subgraph, preserving the core topology of the text semantic space with low overhead and providing a stable, transferable semantic reference for cross-modal geometric distillation.

Finally, we exploit the adversarial anchors to estimate and compensate the drift of old visual prototypes in the raw feature space under the exemplar-free constraint. Specifically, after finishing the current task, we measure the anchor-induced variations of raw visual features before and after adaptation, and use them to transfer the old-class prototypes so that the raw-space decision reference remains consistent with the updated visual encoder. The transferred prototypes are subsequently used as updated visual targets for the next-task DPGD procedure, and as complementary cues for dual-path prediction by fusing cross-modal logits with prototype-based visual logits. This is particularly important due to the modality gap [29], [18] in VLMs, where easy texts alone cannot fully characterize the visual space and discriminative raw visual patterns can provide additional evidence for robust inference. The contributions of this work can be summarized as:

- We reveal that cross-modal semantic-geometry distortion is most pronounced near the vulnerable old-new semantic interface and is closely tied to forgetting, which motivates probing such drift-prone regions via adversarial attacking under the exemplar-free constraint.
- We develop a geometry-preserving distillation framework, combining Anchor-guided Cross-modal Geometry Distillation (ACGD) with Text Semantic Geometry Regularization (TSGR) to stabilize established cross-modal relations and a stable reference frame of textual semantics.
- We further propose a prototype transfer method via anchor-induced drift estimation, and introduce a dual-path prediction that fuses raw visual cues with the cross-modal knowledge for robust inference.
- Extensive experiments on five CL benchmarks demonstrate state-of-the-art performance, with comprehensive analyses validating improved semantic geometry preservation and knowledge transfer.

II. RELATED WORK

A. Foundational Vision-language Models

Large-scale pretrained vision-language models (VLMs) such as CLIP [1] and ALIGN [2] are typically trained on web-scale image-text pairs with contrastive objectives, learning aligned representations between an visual encoder and a textual encoder. This large-scale pretraining yields strong

zero-shot transfer, enabling open-vocabulary recognition via text prompts. For downstream tasks, VLMs can be adapted in a parameter-efficient manner via prompt learning [31], [32], adapter-based tuning [33], [34], and LoRA fine-tuning methods [35], [30]. However, these adaptation methods face severe forgetting challenges in multi-step continual learning scenarios.

B. Continual Learning

Continual learning studies incremental acquisition without catastrophic forgetting. Typical strategies include model expansion [36], [4], [37], knowledge distillation [38], and parameter regularization [39]. These solutions are generally developed for training-from-scratch small backbones, while recent work begins to incrementally inject knowledge into pretrained models. Representative directions include task-deconflicted prompt structures [40], [41], [42], adapter-based designs [43], [13], and lora-based continual learning [44].

Due to the dual-tower cross-modal alignment structure of VLMs and the fact that textual concepts can fully specify visual targets, continual learning on VLMs has become increasingly popular in recent years. The key challenge lies in preserving the inherent cross-modal semantic geometry of VLMs as well as the alignment structure learned from previous tasks. A common direction is to introduce parameter-efficient task components, including learnable prompts [40], [45] and adapters [43], [46], [13]. Beyond these adaptation method, methods exploiting textual priors (e.g., attribute/semantic structures) have shown effectiveness for exemplar-free class-incremental continual learning [8], [3], [9], [16]. However, they typically require an external language expert (e.g., GPT-4) to obtain additional vision-related textual semantic information. Another line updates VLM parameters selectively to reduce generic knowledge loss [47], [48], [11].

Some works have highlighted that preserving the cross-modal geometry of VLMs is crucial for maintaining stable zero-shot transfer ability. Huang et al. [18] argue that narrowing the modality gap during continual updates can be risky to the inherent cross-modal structure, and accordingly propose modality-preservation and modality-compensation strategies. Meanwhile, Suzuki et al. [17] suppress cross-modal structural collapse by measuring and constraining cross-modal representation shifts on reference data. Cross-modal distillation provides another way to preserve cross-modal geometry. Yu et al. [49] propose to leverage stable textual semantic to distill cross-modal and relation distributions for knowledge transfer. Several efforts [19], [50], [51] leverage additional reference datasets for monitoring and distillation to maintain the general capability of VLMs, but such extra data incur non-trivial overhead.

Building upon the above advances and limitations, we propose to explicitly protect the vulnerable cross-modal semantic interface between old and new tasks. Our approach combines cross-modal geometry distillation to preserve the alignment structure acquired in previous tasks with text-semantic geometry regularization, thereby enabling efficient continual learning.

C. Adversarial Attacking on VLMs

VLMs are known to be vulnerable to small, structured perturbations that can rapidly alter image-text alignment, which has spurred both adversarial attack studies and the development of corresponding defenses. Recent studies analyze robustness from text-guided attention [23], hierarchical defense mechanisms [25], and internal feature perturbations [24]. Recent work has investigated concrete adversarial optimization strategies for VLMs. In particular, gradient-based attacks such as the fast gradient sign method (FGSM) [52] and iterative variants (e.g., I-FGSM [53] and projected gradient descent (PGD) [54]) can efficiently craft bounded perturbations that maximize a target objective, such as decreasing image-text similarity for a matched pair or increasing similarity to a target text prompt. Collectively, these studies repeatedly demonstrate that adversarial examples can reveal vulnerable regions in cross-modal geometry. Accordingly, we construct adversarial anchors via Dual-targeted Projected Gradient Descent (DPGD) and enforce cross-modal geometric consistency in these vulnerable regions before and after training, so as to safeguard previously learned alignment knowledge, facilitate transfer, and reduce forgetting.

III. METHODOLOGY

A. Preliminaries

1) *Continual Learning Formulation*: A sequence of task datasets is denoted as $\{\mathcal{D}_1, \mathcal{D}_2, \dots, \mathcal{D}_T\}$. During training on task \mathcal{D}_t , access to previous data $\{\mathcal{D}_1, \dots, \mathcal{D}_{t-1}\}$ is restricted. In class-incremental continual learning, task t introduces a disjoint class set \mathcal{C}_t , and we define $\mathcal{C}_{<t} = \bigcup_{i=1}^{t-1} \mathcal{C}_i$ and $\mathcal{C}_{\leq t} = \mathcal{C}_{<t} \cup \mathcal{C}_t$. The training set for task t only includes:

$$\mathcal{D}_t = \{(\mathbf{x}, y) \mid y \in \mathcal{C}_t\}. \quad (1)$$

2) *CLIP Representations*: As a representative foundational vision-language model (VLM), CLIP [1] consists of a visual encoder $\mathbf{F}(\cdot)$ and a textual encoder $\mathbf{G}(\cdot)$ that map images and texts into an aligned embedding space. The visual encoder is decoupled into a raw extractor and a projection head $\mathbf{P}_{r \rightarrow v}(\cdot)$:

$$\mathbf{r}(\mathbf{x}) = \mathbf{F}^*(\mathbf{x}) \in \mathbb{R}^D, \quad \mathbf{v}(\mathbf{x}) = \mathbf{P}_{r \rightarrow v}(\mathbf{r}(\mathbf{x})) \in \mathbb{R}^d. \quad (2)$$

We use ℓ_2 -normalized features

$$\bar{\mathbf{r}}(\mathbf{x}) = \frac{\mathbf{r}(\mathbf{x})}{\|\mathbf{r}(\mathbf{x})\|_2}, \quad \bar{\mathbf{v}}(\mathbf{x}) = \frac{\mathbf{v}(\mathbf{x})}{\|\mathbf{v}(\mathbf{x})\|_2}. \quad (3)$$

For class c , the text embedding is constructed by prompting (\mathbf{pr}) the textual encoder using the template like “A photo of a *ClassName*.”:

$$\mathbf{u}_c = \frac{\mathbf{G}(\mathbf{pr}.(c))}{\|\mathbf{G}(\mathbf{pr}.(c))\|_2} \in \mathbb{R}^d. \quad (4)$$

CLIP predicts class c by the cross-modal logits $s^{\text{clip}}(\mathbf{x}, c) = \bar{\mathbf{v}}(\mathbf{x})^\top \mathbf{u}_c$, and for a class set $\mathcal{S} \subseteq \mathcal{C}_{\leq t}$, the probability is

$$p^{\text{clip}}(y = c \mid \mathbf{x}; \mathcal{S}) = \frac{\exp(s^{\text{clip}}(\mathbf{x}, c)/\tau)}{\sum_{j \in \mathcal{S}} \exp(s^{\text{clip}}(\mathbf{x}, j)/\tau)}, \quad (5)$$

where τ is a temperature that controls the distribution softness.

3) *Visual Branch*: To complement cross-modal semantics with

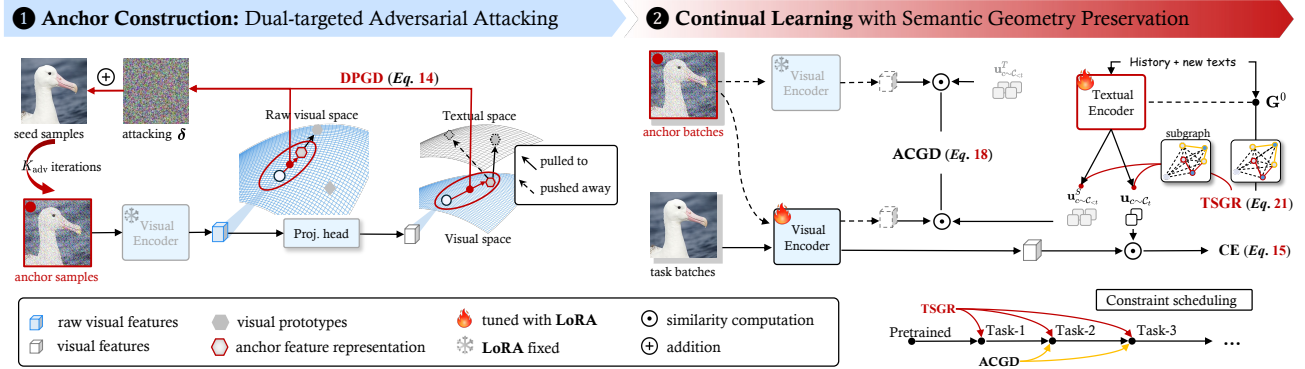


Fig. 3. Overview of proposed **SeGP-CL**. 1) Anchor construction: Dual-targeted projected gradient descent (DPGD) iteratively perturbs seed samples to synthesize adversarial anchors that are simultaneously guided in raw visual space and CLIP feature space. 2) Continual learning: A LoRA-tuned VLM is optimized on task batches with CE loss, while anchor batches and history texts impose semantic-geometry preservation via ACGD and TSGR.

discriminative raw visual patterns, we maintain one normalized raw visual space prototype per class [9], [55], $\mu_c \in \mathbb{R}^D$ with $\|\mu_c\|_2 = 1$. Given $\bar{\mathbf{r}}(\mathbf{x})$, the prototype-branch logits is $s^v(\mathbf{x}, c) = \bar{\mathbf{r}}(\mathbf{x})^\top \mu_c$, and the corresponding probability over \mathcal{S} is

$$p^v(y = c | \mathbf{x}; \mathcal{S}) = \frac{\exp(s^v(\mathbf{x}, c)/\tau)}{\sum_{j \in \mathcal{S}} \exp(s^v(\mathbf{x}, j)/\tau)}. \quad (6)$$

B. Overview

As illustrated in Fig. 3 and Fig. 4, our exemplar-free continual learning framework, **Semantic Geometry Preservation (SeGP-CL)**, comprises three key components. As shown in Fig. 3, before learning task t , we freeze a teacher snapshot $(\mathbf{F}^T, \mathbf{G}^T) = (\mathbf{F}_{t-1}, \mathbf{G}_{t-1})$ and construct a compact anchor set \mathcal{A}_t via Dual-targeted Projected Gradient Descent (DPGD), which perturbs selected seeds from \mathcal{D}_t toward old-class semantics while remaining close to the corresponding old visual prototypes, thereby probing the vulnerable old-new semantic interface. During training, we optimize the student with new-class supervision and preserve prior cross-modal structure by applying Anchor-guided Cross-modal Geometry Distillation (ACGD) on \mathcal{A}_t over $\mathcal{C}_{<t}$, together with a lightweight Text Semantic Geometry Regularization (TSGR) to stabilize the textual semantic reference frame. As shown in Fig. 4, after training, we estimate drift in the raw visual space to transfer old prototypes, and perform dual-path prediction by fusing logits from the CLIP branch and the prototype-based visual branch for robust inference over all seen classes.

C. Anchor Construction

To concentrate supervision on the most vulnerable old-new semantic interface under the exemplar-free setting, we construct a compact set of adversarial anchors that probe the boundary neighborhoods of the old cross-modal geometry. The key idea is to (i) fix a stable semantic reference that faithfully reflects the pre-update old decision geometry, and (ii) start from incoming samples that already exhibit strong affinity to old semantics, so that a small perturbation is sufficient to reach the drift-prone regions. In addition, we adopt iterative projected gradient descent (PGD) [54] as the anchor generator

because it provides an efficient exploration strategy for drift-prone interface neighborhoods under a bounded perturbation budget. Specifically, let $L(\mathbf{x}, c)$ denote a teacher-defined objective whose decrease drives \mathbf{x} toward the old semantic region of class c (in our case, $L = \mathcal{L}_{adv}$ in Eq. (13)). For a single perturbation step Δ with $\|\Delta\|_\infty \leq \gamma$, a first-order approximation gives

$$L(\mathbf{x} + \Delta, c) \approx L(\mathbf{x}, c) + \langle \nabla_{\mathbf{x}} L(\mathbf{x}, c), \Delta \rangle. \quad (7)$$

By Hölder’s inequality, for any feasible Δ ,

$$\langle \nabla_{\mathbf{x}} L, \Delta \rangle \geq -\|\nabla_{\mathbf{x}} L\|_1 \cdot \|\Delta\|_\infty, \quad (8)$$

and the bound is achieved by the sign step $\Delta^* = -\gamma \text{sign}(\nabla_{\mathbf{x}} L)$. Therefore, the sign-gradient update yields the maximum instantaneous decrease of the linearized objective under the ℓ_∞ constraint. Iterating such locally optimal steps efficiently drives seed samples toward and across the teacher-induced old semantic interface, thereby probing the most vulnerable boundary neighborhoods with a small number of iterations.

Concretely, before learning task t , we freeze the model from the previous task as a teacher snapshot $(\mathbf{F}^T, \mathbf{G}^T) = (\mathbf{F}_{t-1}, \mathbf{G}_{t-1})$. This teacher provides pre-update cross-modal semantics, ensuring that anchor construction is guided by the old decision geometry rather than being contaminated by the ongoing update. Given the new-task dataset \mathcal{D}_t , we select a small set of seeds for each old class $c \in \mathcal{C}_{<t}$ by measuring how strongly a new sample is already aligned with the old textual prototype under the teacher. Specifically, for $\mathbf{x} \in \mathcal{D}_t$, we compute the teacher cross-modal similarity

$$Q(\mathbf{x}, c) = \bar{\mathbf{v}}^T(\mathbf{x})^\top \mathbf{u}_c^T, \quad (9)$$

where $\bar{\mathbf{v}}^T(\mathbf{x}) = \frac{\mathbf{v}^T(\mathbf{x})}{\|\mathbf{v}^T(\mathbf{x})\|_2}$, $\mathbf{u}_c^T = \frac{\mathbf{G}^T(\text{pr.}(c))}{\|\mathbf{G}^T(\text{pr.}(c))\|_2}$. We retain the K_{seed} top-ranked samples as \mathcal{I}_c , which serve as initialization points for adversarial perturbation. Intuitively, these seeds capture shared visual patterns that already lie close to old semantics in the teacher embedding space, making them ideal starting points to probe the boundary neighborhoods that are most vulnerable to drift. Starting from a seed $\mathbf{x} \in \mathcal{I}_c$, we

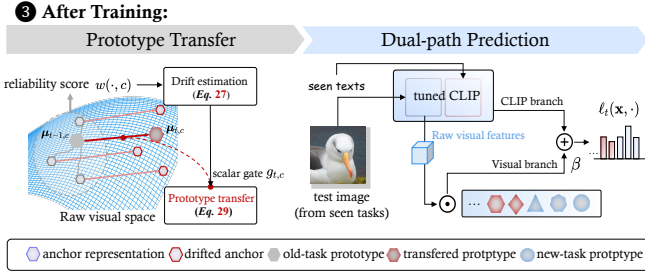


Fig. 4. After training: We estimate raw-space drift and transfer visual prototypes for old classes, then perform dual-path inference by ensembling logits from visual and CLIP branches.

generate an adversarial anchor $\mathbf{x}^{\text{adv}} = \mathbf{x} + \delta$ within an ℓ_∞ budget by optimizing a text-targeted objective:

$$\min_{\|\delta\|_\infty \leq \epsilon} \mathcal{L}_{\text{adv}}(\mathbf{x} + \delta, c), \quad (10)$$

where $\mathcal{L}_{\text{adv}}(\mathbf{x} + \delta, c)$ enforces a relative preference for class c among all old classes, explicitly pushing the perturbed sample toward the teacher's old semantic region:

$$\mathcal{L}_{\text{adv}}(\mathbf{x} + \delta, c) = -\log \frac{\exp(\bar{\mathbf{v}}^T(\mathbf{x} + \delta)^\top \mathbf{u}_c^T / \tau)}{\sum_{j \in \mathcal{C}_{<t}} \exp(\bar{\mathbf{v}}^T(\mathbf{x} + \delta)^\top \mathbf{u}_j^T / \tau)}. \quad (11)$$

However, purely text-targeted perturbations can become unreliable in the presence of the modality gap [29], [18], since the geometric structures of the visual and textual embedding spaces are not perfectly corresponding. As a result, driving an image embedding toward a target text embedding alone may match the direction of textual semantics while deviating from class-consistent visual patterns, yielding unstable or visually implausible anchors. We therefore introduce a visual anchoring term in the raw feature space, which pulls the anchor toward the old raw-space visual prototype of class c :

$$\mathcal{L}_{\text{v-adv}}(\mathbf{x} + \delta, c) = 1 - \bar{\mathbf{r}}^T(\mathbf{x} + \delta)^\top \boldsymbol{\mu}_{t-1, c}, \quad (12)$$

where $\bar{\mathbf{r}}^T(\mathbf{x}) = \frac{\mathbf{r}^T(\mathbf{x})}{\|\mathbf{r}^T(\mathbf{x})\|_2}$. Combining the original objective in Eq. (11) with the visual anchoring term in Eq. (12), we obtain the corrected dual-target objective:

$$\min_{\|\delta\|_\infty \leq \epsilon} \mathcal{L}'_{\text{adv}}(\mathbf{x} + \delta, c) = \mathcal{L}_{\text{adv}}(\mathbf{x} + \delta, c) + \lambda_p \mathcal{L}_{\text{v-adv}}(\mathbf{x} + \delta, c), \quad (13)$$

where λ_p is the correction coefficient. We solve Eq. (13) with standard PGD using step size γ :

$$\delta^{(k+1)} = \Pi_{\|\delta\|_\infty \leq \epsilon} \left(\delta^{(k)} - \gamma \text{sign}(\nabla_{\delta} \mathcal{L}'_{\text{adv}}(\mathbf{x} + \delta^{(k)}, c)) \right), \quad (14)$$

where $\Pi_{\|\delta\|_\infty \leq \epsilon}(\cdot)$ projects onto the ℓ_∞ ball of radius ϵ . Repeating the update for K_{adv} iterations yields anchors that are confidently mapped to old semantics in the teacher embedding space while remaining visually faithful to the incoming distribution. We collect all generated anchors into \mathcal{A}_t , and record each anchor's associated old class for drift estimation and subsequent tasks.

D. Continual Learning with Semantic-Geometry Preservation

Given the anchor set \mathcal{A}_t constructed in Section III-C, we update the student model for task t by jointly balancing new-task acquisition and semantic-geometry preservation. We first optimize standard cross-entropy on the incoming label space \mathcal{C}_t to fit the new supervision:

$$\mathcal{L}_{\text{cls}} = \mathbb{E}_{(\mathbf{x}, y) \sim \mathcal{D}_t} \left[-\log p_t^{\text{clip}}(y | \mathbf{x}; \mathcal{C}_t) \right]. \quad (15)$$

However, optimizing \mathcal{L}_{cls} alone can pull shared visual patterns toward new semantics and induce destructive drift around the old-new interface. We therefore preserve the established cross-modal geometry by distilling the teacher's old-class distribution on anchors $\mathbf{x}^{\text{adv}} \in \mathcal{A}_t$. Here $s^T(\mathbf{x}, c)$ and $s^S(\mathbf{x}, c)$ denote the cross-modal CLIP logits evaluated by the frozen teacher snapshot $(\mathbf{F}^T, \mathbf{G}^T)$ and the current student $(\mathbf{F}^S, \mathbf{G}^S)$, respectively, following the same form as $s^{\text{clip}}(\mathbf{x}, c)$ in Section III-A. Concretely,

$$\begin{aligned} \text{teacher: } s^T(\mathbf{x}, c) &= \left(\frac{\mathbf{v}^T(\mathbf{x})}{\|\mathbf{v}^T(\mathbf{x})\|_2} \right)^\top \underbrace{\left(\frac{\mathbf{G}^T(\text{pr.}(c))}{\|\mathbf{G}^T(\text{pr.}(c))\|_2} \right)}_{\text{snapshot text embedding } \mathbf{u}_c^T}, \\ \text{student: } s^S(\mathbf{x}, c) &= \left(\frac{\mathbf{v}^S(\mathbf{x})}{\|\mathbf{v}^S(\mathbf{x})\|_2} \right)^\top \underbrace{\left(\frac{\mathbf{G}^S(\text{pr.}(c))}{\|\mathbf{G}^S(\text{pr.}(c))\|_2} \right)}_{\text{text embedding } \mathbf{u}_c^S}, \end{aligned} \quad (16)$$

where we have $\forall c \in \mathcal{C}_{<t}$. We then define the temperature-scaled teacher/student distributions using the anchors \mathbf{x}^{adv} on $\mathcal{C}_{<t}$ as

$$\begin{aligned} \text{teacher: } \pi_T^{\tau_A}(c | \mathbf{x}^{\text{adv}}) &= \frac{\exp(s^T(\mathbf{x}^{\text{adv}}, c) / \tau_A)}{\sum_{j \in \mathcal{C}_{<t}} \exp(s^T(\mathbf{x}^{\text{adv}}, j) / \tau_A)}, \\ \text{student: } \pi_S^{\tau_A}(c | \mathbf{x}^{\text{adv}}) &= \frac{\exp(s^S(\mathbf{x}^{\text{adv}}, c) / \tau_A)}{\sum_{j \in \mathcal{C}_{<t}} \exp(s^S(\mathbf{x}^{\text{adv}}, j) / \tau_A)}, \end{aligned} \quad (17)$$

and minimize the Kullback-Leibler (KL) divergence [56] to obtain anchor-guided cross-modal geometry distillation (ACGD):

$$\mathcal{L}_{\text{ACGD}} = \tau_A^2 \mathbb{E}_{\mathbf{x}^{\text{adv}} \sim \mathcal{A}_t} \left[\text{KL}(\pi_T^{\tau_A}(\cdot | \mathbf{x}^{\text{adv}}) \| \pi_S^{\tau_A}(\cdot | \mathbf{x}^{\text{adv}})) \right], \quad (18)$$

where τ_A is a distillation temperature to control the distribution softness.

Beyond local cross-modal constraints, stable continual learning also requires a consistent textual semantic reference frame across tasks. Otherwise, the relative geometry among text concepts may drift and implicitly re-parameterize old semantics even if cross-modal distillation is satisfied. We therefore introduce Text Semantic-Geometry Regularization (TSGR). Concretely, at the beginning of task t , we obtain a fixed teacher \mathbf{G}^0 by resetting the LoRA parameters in the current textual encoder, which recovers a stable textual embedding space shared across tasks. Based on this reference frame, we define a reference subgraph distribution in the teacher text space and match it to the counterpart induced by the current student \mathbf{G}^S . Specifically, we construct the neighbor subgraph under the reference space induced by \mathbf{G}^0 :

for each new class $c \in \mathcal{C}_t$, we first compute the reference text embeddings for all seen classes $j \in \mathcal{C}_{\leq t}$ as $\mathbf{u}_j^0 = \frac{\mathbf{G}^0(\text{pr.}(j))}{\|\mathbf{G}^0(\text{pr.}(j))\|_2}$, and define $\mathcal{N}_k(c)$ as the indices of the k nearest neighbors of \mathbf{u}_c^0 in this reference space (excluding c), i.e., the top- k classes with the largest cosine similarity $(\mathbf{u}_c^0)^\top \mathbf{u}_j^0$. Importantly, $\mathcal{N}_k(c)$ is computed once at the beginning of task t using \mathbf{G}^0 and kept fixed during training, avoiding contamination from the evolving student text space. We then compute the current text embeddings as $\mathbf{u}_j^S = \frac{\mathbf{G}^S(\text{pr.}(j))}{\|\mathbf{G}^S(\text{pr.}(j))\|_2}$, and define the teacher and student subgraph distributions on the same neighbor set as

$$\text{pretrained teacher: } \varphi_0(j | c) = \frac{\exp((\mathbf{u}_c^0)^\top \mathbf{u}_j^0 / \tau_T)}{\sum_{\ell \in \mathcal{N}_k(c)} \exp((\mathbf{u}_c^0)^\top \mathbf{u}_\ell^0 / \tau_T)}. \quad (19)$$

$$\text{student: } \varphi_S(j | c) = \frac{\exp((\mathbf{u}_c^S)^\top \mathbf{u}_j^S / \tau_T)}{\sum_{\ell \in \mathcal{N}_k(c)} \exp((\mathbf{u}_c^S)^\top \mathbf{u}_\ell^S / \tau_T)}. \quad (20)$$

where $j \in \mathcal{N}_k(c)$, and τ_T is the temperature parameter. TSGR minimizes the KL divergence over all selected subgraphs:

$$\mathcal{L}_{\text{GR}} = \frac{1}{|\mathcal{C}_t|} \sum_{c \in \mathcal{C}_t} \text{KL}(\varphi_0(\cdot | c) \| \varphi_S(\cdot | c)). \quad (21)$$

Here, we apply TSGR only to the neighborhood subgraphs rooted at the new classes $c \in \mathcal{C}_t$, rather than enforcing a global relational constraint over all seen concepts. This choice is motivated by both effectiveness and efficiency. First, text embeddings in VLM-based continual learning are typically more stable than visual ones [57], and the optimization at task t primarily perturbs the newly introduced class texts and their nearby semantic neighborhood; thus, geometric distortion is more likely to arise locally around these new nodes. Second, TSGR is implemented via local k -NN subgraph matchings, whose cost scales with the number of rooted subgraphs. Restricting the constraint to $|\mathcal{C}_t|$ new-class roots yields $\mathcal{O}(|\mathcal{C}_t|k)$ similarity terms per step, which is substantially cheaper than the global $\mathcal{O}(|\mathcal{C}_{\leq t}|k)$ overhead in class-incremental learning where $|\mathcal{C}_t| \ll |\mathcal{C}_{\leq t}|$.

Combining the above components, the overall objective for task t is given by

$$\min_{\theta_{\text{LoRA}}^S} \mathcal{L}_{\text{CL}}^t = \mathcal{L}_{\text{cls}} + \lambda_{\text{ACGD}} \mathcal{L}_{\text{ACGD}} + \lambda_{\text{GR}} \mathcal{L}_{\text{GR}}, \quad (22)$$

where θ_{LoRA}^S denotes the LoRA parameters inserted into the student model $(\mathbf{F}^S, \mathbf{G}^S)$ at task t .

E. After Training

1) *Anchor-induced Prototype Transfer*: After completing training, we obtain the updated model $(\mathbf{F}_t, \mathbf{G}_t)$ and update the visual prototypes to keep the raw-space decision reference consistent with the adapted visual encoder. For the newly introduced classes $c \in \mathcal{C}_t$, we directly estimate prototypes from the available task- t training data:

$$\boldsymbol{\mu}_{t,c} = \frac{\sum_{(\mathbf{x},y) \in \mathcal{D}_t, y=c} \bar{\mathbf{r}}_t(\mathbf{x})}{\left\| \sum_{(\mathbf{x},y) \in \mathcal{D}_t, y=c} \bar{\mathbf{r}}_t(\mathbf{x}) \right\|_2}, \quad \forall c \in \mathcal{C}_t, \quad (23)$$

where $\bar{\mathbf{r}}_t(\mathbf{x}) = \frac{\mathbf{r}_t(\mathbf{x})}{\|\mathbf{r}_t(\mathbf{x})\|_2}$. For the old classes $c \in \mathcal{C}_{< t}$, exemplar-free CL prevents recomputing prototypes from old

data. Instead, we estimate how the raw visual prototypes shift using the adversarial anchors. Inspired by representation-drift compensation works [58], [59], we note that each anchor $\mathbf{x}^{adv} \in \mathcal{A}_t$ is generated by the frozen teacher to lie close to old semantics while remaining visually faithful (Section III-C). Therefore, the feature discrepancy of these anchors under the teacher and the updated encoders provides a direct probe of anchor-induced drift in the raw visual space. Concretely, for each old class $c \in \mathcal{C}_{< t}$, let $\mathcal{A}_t^c \subseteq \mathcal{A}_t$ denote the anchors associated with class c . For $\mathbf{x}^{adv} \in \mathcal{A}_t^c$, based on the normalized raw visual features $\bar{\mathbf{r}}^T(\mathbf{x}^{adv}) = \frac{\mathbf{r}^T(\mathbf{x}^{adv})}{\|\mathbf{r}^T(\mathbf{x}^{adv})\|_2}$, and $\bar{\mathbf{r}}_t(\mathbf{x}^{adv}) = \frac{\mathbf{r}_t(\mathbf{x}^{adv})}{\|\mathbf{r}_t(\mathbf{x}^{adv})\|_2}$ before/after task- t learning, we define the raw-space displacement of each anchor:

$$\mathbf{d}_t(\mathbf{x}^{adv}) = \bar{\mathbf{r}}_t(\mathbf{x}^{adv}) - \bar{\mathbf{r}}^T(\mathbf{x}^{adv}). \quad (24)$$

Considering that not all anchors are equally reliable for characterizing the drift of a specific old class, we weight each anchor by its proximity to the previous prototype under the teacher in the raw visual space, using its similarity as a reliability score:

$$a(\mathbf{x}^{adv}, c) = \bar{\mathbf{r}}^T(\mathbf{x}^{adv})^\top \boldsymbol{\mu}_{t-1,c}. \quad (25)$$

We then normalize the scores within \mathcal{A}_t^c to obtain the anchor weights:

$$w(\mathbf{x}^{adv}, c) = \frac{a(\mathbf{x}^{adv}, c)}{\sum_{\mathbf{z} \in \mathcal{A}_t^c} a(\mathbf{z}, c)}. \quad (26)$$

This gives a class-wise drift direction as the weighted average displacement:

$$\Delta_{t,c} = \sum_{\mathbf{x}^{adv} \in \mathcal{A}_t^c} w(\mathbf{x}^{adv}, c) \mathbf{d}_t(\mathbf{x}^{adv}). \quad (27)$$

Note that $\Delta_{t,c}$ estimates the anchor-induced translation for class c . We further modulate its magnitude by the overall anchor-prototype proximity under the teacher:

$$g_{t,c} = \frac{1}{|\mathcal{A}_t^c|} \sum_{\mathbf{x}^{adv} \in \mathcal{A}_t^c} \bar{\mathbf{r}}^T(\mathbf{x}^{adv})^\top \boldsymbol{\mu}_{t-1,c}, \quad \forall c \in \mathcal{C}_{< t}. \quad (28)$$

Finally, we transfer old prototypes via

$$\boldsymbol{\mu}_{t,c} = \frac{\boldsymbol{\mu}_{t-1,c} + g_{t,c} \Delta_{t,c}}{\|\boldsymbol{\mu}_{t-1,c} + g_{t,c} \Delta_{t,c}\|_2}. \quad (29)$$

2) *Dual-path Prediction*: At inference time after task t , we combine two complementary decision signals: (i) the cross-modal matching scores produced by CLIP, which inherit the pretrained vision-language semantics, and (ii) the raw-space prototype scores, which capture discriminative visual cues that may not be fully represented by textual embeddings under the modality gap [9], [55]. This dual-path design is particularly suitable for exemplar-free continual learning, where preserving cross-modal semantics is crucial while a lightweight visual reference can further improve robustness. Given a test image \mathbf{x} and a candidate class $c \in \mathcal{C}_{\leq t}$, we compute the CLIP branch score and the prototype branch score as

$$s_t^{\text{clip}}(\mathbf{x}, c) = \bar{\mathbf{v}}_t(\mathbf{x})^\top \mathbf{u}_{t,c}, \quad s_t^v(\mathbf{x}, c) = \bar{\mathbf{r}}_t(\mathbf{x})^\top \boldsymbol{\mu}_{t,c}, \quad (30)$$

TABLE I
COMPARISON WITH DIFFERENT METHODS USING A CLIP-ViT-B/16 BACKBONE.

Method	Publication	Replay	CIFAR100 ⁽¹⁰⁾		ImageNet-R ⁽¹⁰⁾		ImageNet-Sub ⁽¹⁰⁾		CUB-200 ⁽¹⁰⁾		UCF ⁽¹⁰⁾	
			Avg	Last	Avg	Last	Avg	Last	Avg	Last	Avg	Last
SLCA [12]	<i>ICCV'23</i>		80.5	67.6	75.9	70.4	78.6	59.9	73.3	60.4	–	–
L2P++ [40]	<i>CVPR'22</i>		81.9	73.1	81.7	76.0	80.5	67.2	71.9	63.0	–	–
DualPrompt [41]	<i>ECCV'22</i>		81.5	72.5	82.0	75.8	80.7	67.4	71.7	63.1	91.0	84.9
CODA Prompt [42]	<i>CVPR'23</i>		77.0	62.3	78.0	67.5	64.1	34.8	66.6	50.9	87.7	82.3
Aper-Adapter [46]	<i>IJCV'24</i>		75.8	65.5	78.7	71.4	85.8	76.4	–	–	–	–
Continual-CLIP [60]	–		–	66.7	–	72.0	–	75.4	–	51.2	–	65.2
CLAP [61]	<i>NeurIPS'24</i>	✓	86.1	78.2	85.8	80.0	87.8	79.2	85.8	80.7	91.4	86.4
MoE-Adapter [13]	<i>CVPR'24</i>		85.4	78.4	85.3	80.8	86.4	76.7	–	–	–	–
RAPF [10]	<i>ECCV'24</i>		86.2	79.0	85.6	80.3	87.5	80.2	82.7	76.2	92.5	87.5
PROOF [3]	<i>TPAMI'25</i>	✓	84.9	76.3	82.8	77.1	84.7	72.5	83.1	75.5	93.6	88.9
CLG-CBM [15]	<i>CVPR'25</i>		84.9	76.9	–	–	86.0	78.5	82.9	77.8	–	–
DMNSP [57]	<i>ICCV'25</i>		87.1	79.9	82.7	76.2	85.0	76.1	–	–	–	–
ENGINE [9]	<i>ICCV'25</i>		82.1	73.1	84.4	77.0	–	–	83.9	76.2	95.0	90.1
MG-CLIP [18]	<i>ICCV'25</i>		87.0	80.6	87.6	82.7	87.3	78.4	80.6	72.0	–	–
DesCLIP [14]	<i>TMM'26</i>		85.6	78.7	85.1	78.7	86.4	77.8	80.7	72.2	–	–
SeGP-CL-onlyCLIP			88.2	83.2	87.4	83.9	88.7	78.8	83.0	74.8	91.4	88.9
SeGP-CL (Ours)			89.8	84.6	88.9	84.8	89.9	80.5	85.4	80.1	95.9	92.8

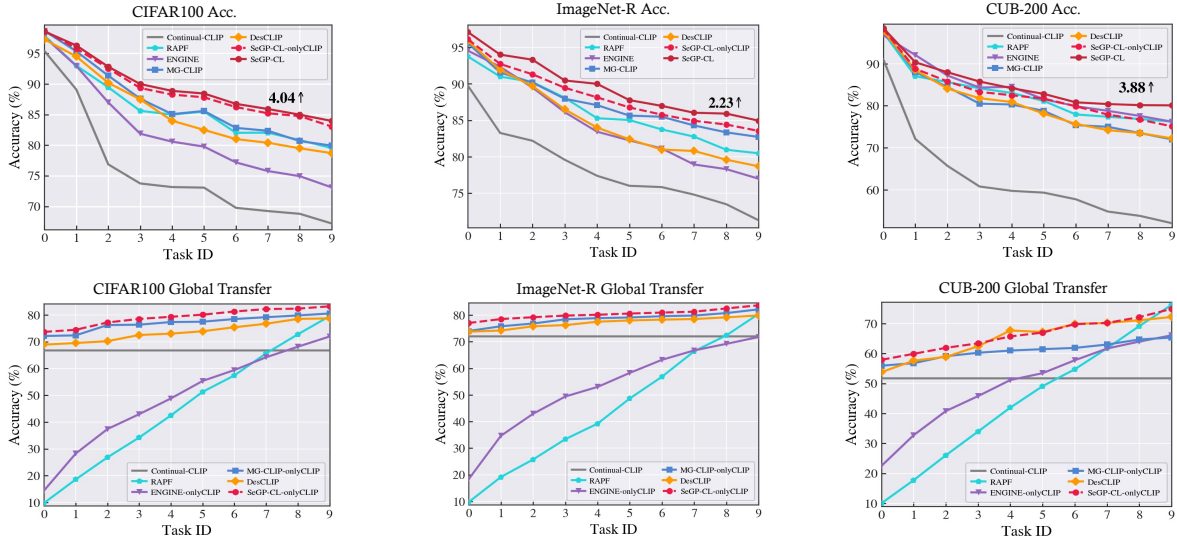


Fig. 5. Comparison with state-of-the-art CL methods in terms of per-task accuracy and global transfer. All results are achieved on the same CLIP ViT-B/16 backbone.

where $\bar{\mathbf{v}}_t(\mathbf{x}) = \frac{\mathbf{v}_t(\mathbf{x})}{\|\mathbf{v}_t(\mathbf{x})\|_2}$ and $\mathbf{u}_{t,c} = \frac{\mathbf{G}_t(\text{pr.}(c))}{\|\mathbf{G}_t(\text{pr.}(c))\|_2}$ denote the normalized image and class-text embeddings of the adapted CLIP, and $\bar{\mathbf{r}}_t(\mathbf{x})$ and $\boldsymbol{\mu}_{t,c}$ are the normalized raw visual feature and the corresponding class prototype (Sec. III-A). We then fuse the two branches by a weighted logit ensembling:

$$\ell_t(\mathbf{x}, c) = s_t^{\text{clip}}(\mathbf{x}, c) + \beta s_t^v(\mathbf{x}, c), \quad c \in \mathcal{C}_{\leq t}, \quad (31)$$

and predict the label by

$$\hat{y} = \arg \max_{c \in \mathcal{C}_{\leq t}} \ell_t(\mathbf{x}, c). \quad (32)$$

IV. EXPERIMENTS

A. Setup

1) *Benchmark*: Our experiments for VLM-based continual learning are conducted on the common CL benchmark, including CIFAR100 [62], ImageNet-Sub [21], CUB-200 [63], ImageNet-R [64], and UCF101 [65].

2) *Metrics*: To evaluate VLM-based continual learning, we report two primary metrics: *Last* and *Avg*. *Last* denotes the average classification accuracy over all seen classes after training on the final task, while *Avg* is the mean incremental accuracy averaged over tasks. To further characterize knowledge transfer and retention, we also report *Forward Transfer* (FWT), *Backward Transfer* (BWT), and *Forgetting*. Following the standard protocol, let $R_{i,j}$ be the test accuracy on task j after completing training on task i . Then

$$\text{BWT} = \frac{1}{t-1} \sum_{j=1}^{t-1} (R_{t,j} - R_{j,j}), \quad \text{FWT} = \frac{1}{t-1} \sum_{j=2}^t R_{j-1,j}, \quad (33)$$

and the *Forgetting* is computed as

$$\text{Forgetting} = \frac{1}{t-1} \sum_{j=1}^{t-1} \left(\max_{i \leq t} R_{i,j} - R_{t,j} \right). \quad (34)$$

TABLE II

COMPARISON ON FORWARD TRANSFER (FWT), BACKWARD TRANSFER (BWT) AND FORGETTING (F) OF THE GLOBAL VISUAL-TEXT MATCHING.

Methods(onlyCLIP)	CIFAR100			ImageNet-R		
	FWT \uparrow	BWT \uparrow	F \downarrow	FWT \uparrow	BWT \uparrow	F \downarrow
ENGINE	0	-10.9	7.9	0	-7.0	7.1
RAPF	0	-8.9	8.5	0	-6.1	6.6
DesCLIP	68.7	-2.1	6.5	74.9	-1.0	1.7
MG-CLIP	70.2	-3.9	4.9	76.2	-0.01	0.88
SeGP-CL	72.3	-0.43	0.9	77.0	+0.03	0.32

3) *Competitors*: We compare our method against baseline and state-of-the-art methods for continual learning. These include (i) **Vision-based CL approaches**: L2P++ [40], DualPrompt [41], CODA Prompt [42] and SLCA [12]; (ii) **VLM-based approaches**: ContinualCLIP [60] (zero-shot baseline), PROOF [3], CLAP [61], MoE-Adapters [13], RAPF [10], CLG-CBM [15], DMNSP [57], ENGINE [9], DesCLIP [14], and MG-CLIP [18].

4) *Implementation Details*: All experiments are conducted on two NVIDIA GeForce RTX 4090 GPUs. We adopt the pre-trained CLIP [1] ViT-B/16 from OpenAI as the backbone. To ensure a fair comparison, all methods are built upon the same pre-trained backbones.

The model is trained for 10 epochs on each incremental task. We use stochastic gradient descent (SGD) [66] with a cosine learning-rate decay schedule, a batch size of 128, and an initial learning rate of 0.001. Following [18], we insert LoRA [35] into both the visual and textual encoders of CLIP by reparameterizing the Transformer attention projection matrices and the linear layers in the Feedforward Network (*FFN*). During continual adaptation, we freeze the LoRA down-projection matrices (*A*) and only update the up-projection matrices (*B*). For DPGD, we set $\lambda_p = 0.5$ to form the corrected objective \mathcal{L}'_{adv} , and run $K_{adv} = 10$ iterations with step size $\gamma = 1.5 \times 10^{-3}$. For each old prototype, we select $K_{seed} = 5$ seed samples for attack and use the 5 anchors for ACGD. During training, we set the anchor batch size to 32 for distillation. For the distillation temperatures, we use $\tau_A = 20$ and $\tau_T = 0.05$. The loss weights are set to $\lambda_{ACGD} = 5$ and $\lambda_{GR} = 1$. For TSGR, the k in the k -NN subgraph is set to 10. For logit ensembling at inference, we set the visual-branch coefficient to $\beta = 0.5$.

B. Comparison with State-of-the-art Methods

Table I summarizes the results on five benchmarks in terms of *Avg* and *Last*. Compared with both vision-only continual learning baselines SLCA [12], DualPrompt [41], L2P++ [40] and VLM-oriented approaches RAPF [10], ENGINE [9], and MG-CLIP [18]), our method consistently achieves the best overall performance without any data replay. In particular, on CIFAR100, **SeGP-CL** improves the *Last* accuracy from 80.6 (MG-CLIP) to 84.6 (+4.0), and on CUB-200 it boosts *Last* from 76.2 (RAPF) to 80.1 (+3.9). Notably, even under the *onlyCLIP* setting (relying purely on CLIP vision-text matching without additional vision-branch predictors), our method remains highly competitive and still surpasses prior methods

TABLE III

COMPARISON ON DISTILLATION SCHEMES AND DATA SOURCES.

Schemes	Source	#Samples	Δ Avg	Δ Last
Naive (baseline)	–	–	(84.6)	(77.0)
ZSCL [19]	w/ Ref.	28K in [20]	+1.0	+1.9
DualTeacher [50]	w/ Ref.	100K in [21]	+0.7	+1.5
GIFT [26]	w/ Syn.	5 /old class	+1.4	+2.5
GIFT [26]	w/ Syn.	100 /old class	+1.5	+2.7
SGCL [49]	w/ New	500 /new class	+1.8	+2.5
CGD	w/ New	500 /new class	-0.8	-0.5
CGD	w/ Seed	5 /old class	+1.2	+3.1
CGD	w/ Adv. anchors	5 /old class	+3.3	+5.8

TABLE IV

ABLATION ON KEY COMPONENTS. ‘PT’ DENOTES USING PROTOTYPE TRANSFER AND ‘V.’ DENOTES USING AN ADDITIONAL VISUAL BRANCH FOR PREDICTION.

Components				CIFAR100		UCF	
w/ \mathcal{L}_{ACGD}	w/ \mathcal{L}_{GR}	w/ PT	w/ V.	<i>Last</i>	F \downarrow	<i>Last</i>	F \downarrow
–	–	–	–	77.0	10.9	84.4	10.7
✓	–	–	–	81.7	5.8	88.2	6.6
✓	✓	–	–	82.8	4.7	88.0	6.9
✓	✓	✓	–	83.2	4.3	88.9	6.3
✓	✓	✓	✓	84.6	4.5	92.8	6.8

that typically depend on extra visual-branch components (e.g. ENGINE, MG-CLIP). Beyond these, Fig. 5(Upper) provides a per-task comparison across the entire incremental process, where our approach maintains the highest seen-task average accuracy and exhibits the smallest degradation on previous tasks, suggesting substantially reduced forgetting.

Moreover, since CLIP is endowed with strong zero-shot ability, we explicitly assess whether such inherent visual-textual cognition can be progressively accumulated during downstream incremental adaptation. Specifically, we adopt a global evaluation protocol: after each incremental stage, we evaluate all test samples from all tasks, and predict each sample against the entire class set solely via CLIP’s image-text matching, without any auxiliary vision-side classifier. As shown in Fig. 5(Bottom), under this global transfer setting, our **SeGP-CL** exhibits stable and monotonic improvement. In contrast, recent approaches such as RAPF and ENGINE, which rely on task-specific components, may perturb the shared vision-language embedding space and thereby undermine global image-text matching, resulting in weakened forward transfer. In other words, our method truly incrementally accumulates downstream knowledge from the pretrained state through controlled adaptation, rather than merely reorganizing. These observations are further supported by the metrics in Table II, where our method achieves the strongest *Forward Transfer* (FWT), *Backward Transfer* (BWT), and the lowest *Forgetting* (F), demonstrating the effectiveness of preserving cross-modal semantic geometry.

C. Comparison with Distillation Schemes

We compare representative distillation schemes and distillation data sources under an identical CLIP two-tower fine-tuning backbone to assess their effectiveness in preserving cross-modal knowledge on CIFAR100 (Table III). We include ZSCL [19] and DualTeacher [50], both of which regularize

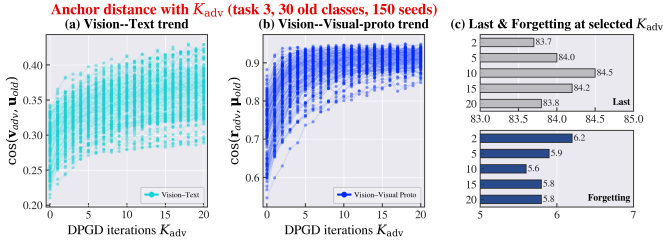


Fig. 6. Effect of adversarial iterations K_{adv} . We visualize the distance evolution of anchor construction across DPGD iterations in (a) CLIP embedding space and (b) raw visual feature space, and report the corresponding continual learning performance in (c).

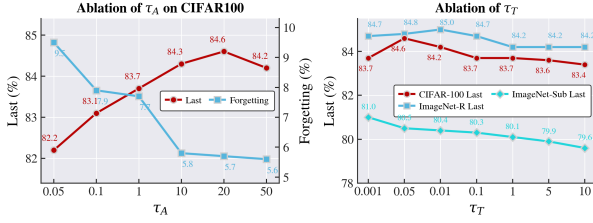


Fig. 7. Ablation of distillation temperature τ_A and τ_T .

CLIP with additional reference data to stabilize the vision–language geometry and visual representations. Specifically, ZSCL distills cross-modal relations on the Conceptual Captions 12M (CC12M) [20] validation set as a task-agnostic reference corpus, while DualTeacher introduces an extra ImageNet reference set to impose representation-level constraints. We further consider variants that distill on either the incoming new-task data or a small seed set, and we denote our cross-modal geometry distillation in Sec. III-D as CGD. Overall, reference-based distillation consistently mitigates forgetting, whereas distilling directly on new-task data is detrimental and markedly impedes learning of new classes. In contrast, seeds and our adversarial-anchor strategy explicitly target vulnerable cross-modal semantic boundaries of old classes. Adversarial anchors provide the strongest gains, improving over the Naive baseline (LoRA fine-tune) by +5.8 in *Last*. In addition, we compare with SGCL [49], which is conceptually related to our geometry-aware distillation. SGCL builds a semantic reference by using a fixed text-encoder reference frame to generate semantic pseudo-labels, and learns both the cross-modal reference distribution and the text-modality relational distribution using only new-task images. Empirically, SGCL performs much better than new-data distillation variant, indicating the benefit of introducing a stable semantic reference even without exemplars.

Beyond these baselines, we further compare a recent synthetic-data-based VLM distillation approach, GIFT [26], which leverages Stable Diffusion [67] to synthesize old-class-related images from textual prompts. However, due to the lack of neighborhood targeting and the domain gap between synthesized samples and real old-task data, its improvement on CIFAR100 is limited.

D. Ablation Study

1) *Component Effectiveness*: We analyze how each key component of our proposed SeGP-CL contributes to the

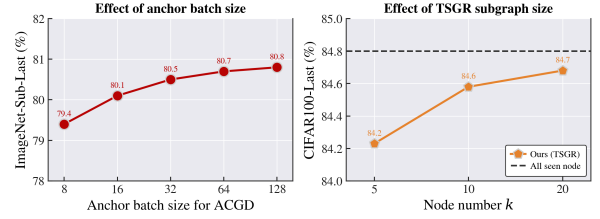


Fig. 8. Ablation of anchor batch size and number of subgraph node.

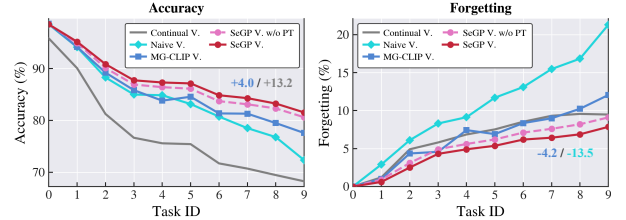


Fig. 9. Evaluation of cross-modal transfer robustness on CIFAR100. We annotate the gains in *Last* accuracy and *Forgetting* relative to the baselines.

continual learning performance, as summarized in Table IV. We observe that ACGD substantially alleviates forgetting of previously learned knowledge. Moreover, TSGR and Prototype Transfer (PT) further stabilize the semantic geometry of the VLM, leading to improved knowledge retention and overall performance.

2) *Anchor Construction Analysis*: We further investigate the sensitivity of our approach to the anchor construction process on CIFAR-100, as shown in Fig. 6. By running DPGD for multiple iterations, we progressively construct anchor samples that move within the local neighborhood and gradually approach the old-class semantic prototypes from two references: the text embedding and the raw-visual prototype. Notably, due to the modality gap [29], PGD guided by the raw-visual prototype typically converges faster, whereas the text-prototype branch exhibits more pronounced oscillations during optimization. Our results also suggest that more iterations are not always better: making anchors arbitrarily close to the old prototypes does not necessarily yield larger distillation gains. In particular, we observe the best trade-off around $K_{adv} = 10$, which achieves the highest *Last* accuracy and the lowest Forgetting. When further increasing K_{adv} , both *Last* and *Forgetting* deteriorate. This phenomenon highlights the necessity of protecting cross-modal geometry specifically in semantically vulnerable neighborhoods, rather than enforcing overly aggressive prototype attraction.

3) *Analysis of Distillation Configurations*: We further examine the distillation configurations used in continual learning. As shown in Fig. 7, we vary the distillation temperatures τ_A and τ_T to study their effects. We find that ACGD benefits from a relatively high temperature, $\tau_A = 20$, which achieves the lowest forgetting and the highest *Last* accuracy. This indicates that anchor-guided distillation is more effective when it prioritizes preserving the global cross-modal geometry (larger τ_A) instead of over-emphasizing overly sharp, local relations (smaller τ_A). In contrast, TSGR favors a lower temperature τ_T , highlighting the importance of maintaining a compact and semantically relevant local relational subgraph in the text space

TABLE V
CROSS-SCENARIO ROBUSTNESS EVALUATION.

Method	CIFAR-Last	Food101	Oxford-Pets	ImageNet-full(1K)
<i>zero-shot</i> CLIP	66.7	85.1	87.6	64.4
PROOF	76.3	9.8	22.8	11.2
RAPF	79.0	17.2	28.6	15.2
MoE-Adapter	78.4	82.9	84.1	66.0
SPU	77.0	84.3	85.9	62.4
MG-CLIP	80.6	85.7	88.2	67.3
SeGP-CL w/o TSGR	84.2	82.1	85.2	62.4
SeGP-CL	84.6	84.5	87.7	67.6

TABLE VI
COMPARISON ON TRAINABLE PARAMETERS AND TIME COST. K, V REPRESENTS THE *key/value* ATTENTION PROJECTION WEIGHTS. UNDERLINED VALUES INDICATE THE BASELINE AVERAGE TIME.

Setting		CIFAR-Last	#Trainable Params	Avg Time(ms) / Iter.
Ours (rank=8)	K, V	83.1	0.25M	<u>330+53</u>
	FFN	82.3	0.61M	<u>401+69</u>
	$K, V+FFN$	83.4	0.86M	<u>410+74</u>
Ours (rank=32)	K, V	83.9	0.98M	<u>339+55</u>
	FFN	83.1	2.46M	<u>419+68</u>
	$K, V+FFN$	84.6	3.44M	<u>424+79</u>
MG-CLIP (rank=8)		80.6	0.54M	333
MG-CLIP (rank=32)		80.8	2.02M	343
ZSCL (full FT)		74.2	149.6M	4205
MoE-Adapter		78.4	13.35M	1679
DMNSP		79.9	7.8M	-
CLAP		78.2	9.45M	-

during continual updates.

In addition, we conduct detailed ablation studies on (i) the anchor batch size for distillation and (ii) the number of k -NN subgraph nodes. In addition, we perform ablations on (i) the anchor batch size used for distillation and (ii) the neighborhood size k in TSGR, as summarized in Fig. 8. We find that ACGD remains robust even with a small anchor batch size (e.g., 16 or 32), while larger batches further strengthen cross-modal geometry preservation. For TSGR, enforcing the constraint on a compact k -NN neighborhood around each new-class text embedding is sufficient to regularize semantic relations effectively. In particular, using $k=10$ neighbors per new-class node achieves performance close to a global constraint over all seen nodes, while substantially reducing the computational overhead.

E. Robustness Evaluation

1) *Cross-scenario Robustness Evaluation*: Preserving the generic cross-modal zero-shot capability of VLMs while continually adapting to downstream tasks is crucial [11], [18], [19]. Following [18], we evaluate the zero-shot transferability of CLIP after continual tuning on several cross-domain benchmarks. Specifically, we include Food-101 [68], Oxford-Pets [69], and ImageNet-full (1K) [21] to assess the intrinsic cross-modal ability of the model after completing all 10 CL stages on CIFAR100. As shown in Table V, while achieving the best CL performance on CIFAR100, our method still maintains zero-shot accuracy comparable to, and even slightly higher than, the original *zero-shot* CLIP on Food-101, Oxford-Pets, and ImageNet-full. This suggests that our adaptation preserves the pretrained cross-modal alignment structure and enables downstream knowledge to be accumulated on top of CLIP, instead of being re-organized by task-specific auxiliary

components. In contrast, methods that introduce incremental-task-specific modules (e.g., PROOF, RAPF, and ENGINE) tend to re-route predictions through task-dependent heads, which can distort the shared vision-language embedding space and weaken the global image-text matching capability, leading to notably degraded cross-scenario robustness.

2) *Cross-modal Transfer Robustness*. While SeGP-CL is primarily designed to preserve underlying cross-modal and text-semantic geometry, we find that this stabilization can transfer back to the visual modality and improve purely visual-branch continual adaptation (predict as Eq. 6) as well. Intuitively, by anchoring the student updates with ACGD and maintaining a stable textual semantic reference frame via TSGR, the visual encoder is guided to update along directions that remain compatible with the pretrained vision-language structure, which in turn yields more stable and discriminative raw visual representations. Together with the after-training prototype transfer (PT), these cross-modal constraints provide an implicit but effective regularization for the visual branch. We refer to this phenomenon as *cross-modal transfer robustness*, namely, the ability of cross-modal geometry preservation to induce robust continual adaptation in the visual branch even when it is evaluated in a unimodal manner. As shown in Fig. 9, the visual-branch variant (SeGP V.) consistently outperforms naive fine-tuning and the visual branch of MG-CLIP (MG-CLIP V.) [18]. More importantly, it achieves an exceptionally low forgetting rate, even lower than a frozen CLIP visual-classifier baseline (Continual V.). These results indicate that the gains brought by SeGP are not confined to cross-modal matching, but can be effectively distilled into a stronger and more stable visual representation stream, providing empirical support for our dual-path prediction that fuses cross-modal logits with prototype-based visual cues.

F. Computational Cost

Table VI summarizes the computational overhead of our method in terms of trainable parameters and runtime. By fine-tuning CLIP with LoRA, our approach achieves stable continual adaptation with substantially fewer trainable parameters, resulting in a markedly smaller footprint than MoE-Adapter [13] and ZSCL [19], and also remaining more lightweight than CLAP [61] and DMNSP [57]. Compared with standard fine-tuning baselines, the proposed distillation introduces only a minor training-time overhead: the overall training time increases by less than 20%, while still being noticeably faster than MoE-Adapter [13] and ZSCL [19], highlighting the plug-and-play nature of our framework. At inference time, our method incurs a negligible additional cost beyond the original CLIP backbone (17.56 GFLOPs), since the auxiliary visual branch contributes only 0.00013 GFLOPs.

G. Visualization

As shown in Fig. 10, we visualize the optimization trajectories starting from seed samples selected from the new-task data, and illustrate how the adversarial perturbations δ evolve across DPGD iterations. As the iterations proceed, the perturbations gradually exhibit structured textures. Visually,

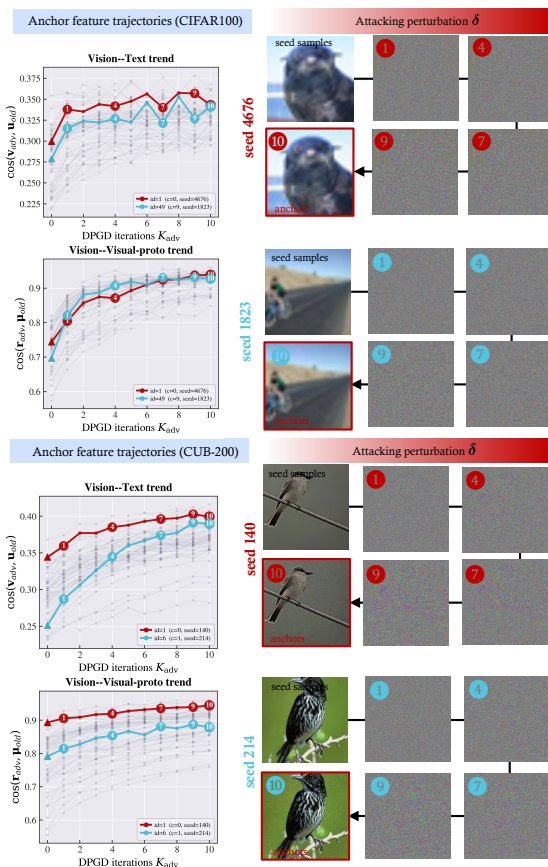


Fig. 10. DPGD optimization trajectories of adversarial anchors in visual-textual (CLIP) space and raw visual space.

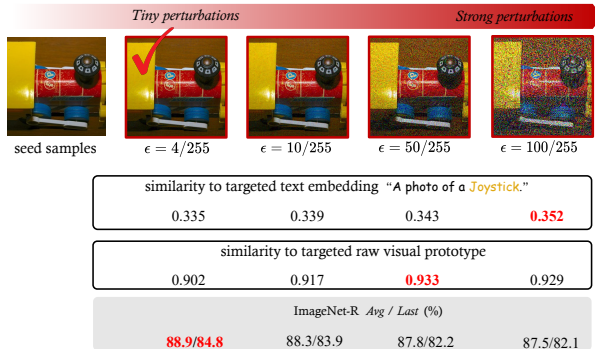


Fig. 11. Effect of perturbation budget on adversarial anchors. We visualize anchors generated with increasing ℓ_∞ radius ϵ , and report their similarities to the targeted old text embedding and raw visual prototype, together with the resulting ImageNet-R CL performance.

the resulting adversarial samples remain almost indistinguishable from the original new-task images. Nevertheless, DPGD progressively shifts their semantics from the semantic neighborhood of the new classes toward the semantic region of previously learned classes, thereby covering the vulnerable semantic neighborhood identified in prior tasks.

In addition, Fig. 11 visualizes the effects of different perturbation budgets. Notably, under larger radii, DPGD can produce anchors that appear semantically closer to the old-class prototypes, as evidenced by higher vision-text similarity and higher vision-visual-prototype similarity. However,

distillation on these large-radius anchors yields markedly worse performance than the tiny-perturbation setting (e.g., $\epsilon = 4/255$). This observation further supports our claim that mining anchors via small, fast perturbations within the semantic neighborhood is crucial for effective cross-modal geometry preservation.

H. Limitations

Although our framework does not store any real exemplar images from previous tasks, it still maintains a lightweight historical memory in the form of raw texts and raw visual prototypes. This introduces additional, albeit modest, storage and computation overhead for anchor construction and geometry regularization. Moreover, our study focuses on robust transfer and preservation of established cross-modal knowledge in class-incremental continual learning, rather than cooperative learning across multiple independent tasks or domains [19], [70]. Finally, the effectiveness of the semantic-relevance structure depends on the quality of prompt-template, and the current design may be limited under severely out-of-distribution scenarios where vision-language relations deviate substantially from the pretrained alignment.

V. CONCLUSIONS

Current continual learning of vision-language models (VLMs) often update the visual encoder under new-task supervision without explicitly protecting the cross-modal semantic geometry inherited from pretraining or previous tasks. Empirically, such unprotected updates are often reflected by an amplified geometric drift around the old-new cross-modal semantic interface, i.e., in the vulnerable neighborhoods where shared visual patterns are most susceptible to being re-interpreted by new-task texts, which accelerates forgetting. In this work, we propose SeGP-CL, a concise framework for semantic geometry preservation during continual learning. Specifically, we construct a compact set of adversarial anchors via DPGD to probe drift-prone neighborhoods, and introduce anchor-guided cross-modal geometry distillation together with a lightweight text semantic-geometry regularization to stabilize the textual reference frame during adaptation. After training, we further perform anchor-induced prototype transfer and adopt a dual-path inference scheme that fuses cross-modal and prototype cues for robust prediction. Extensive experiments validate the effectiveness of SeGP-CL, consistently accumulating downstream-task knowledge and reducing forgetting compared with existing VLM-based continual learning baselines.

REFERENCES

- [1] A. Radford, J. W. Kim, C. Hallacy, A. Ramesh, G. Goh, S. Agarwal, G. Sastry, A. Askell, P. Mishkin, J. Clark *et al.*, "Learning transferable visual models from natural language supervision," in *International conference on machine learning*. PMLR, 2021, pp. 8748–8763.
- [2] C. Jia, Y. Yang, Y. Xia, Y.-T. Chen, Z. Parekh, H. Pham, Q. Le, Y.-H. Sung, Z. Li, and T. Duerig, "Scaling up visual and vision-language representation learning with noisy text supervision," in *International conference on machine learning*. PMLR, 2021, pp. 4904–4916.
- [3] D.-W. Zhou, Y. Zhang, Y. Wang, J. Ning, H.-J. Ye, D.-C. Zhan, and Z. Liu, "Learning without forgetting for vision-language models," *IEEE Transactions on Pattern Analysis and Machine Intelligence*, vol. 47, no. 6, pp. 4489–4504, 2025.

- [4] D.-W. Zhou, Q.-W. Wang, H.-J. Ye, and D.-C. Zhan, "A model or 603 exemplars: Towards memory-efficient class-incremental learning," in *The Eleventh International Conference on Learning Representations*, 2022.
- [5] Z. Qiu, Y. Xu, C. He, F. Meng, L. Xu, Q. Wu, and H. Li, "Mingle: Mixture of null-space gated low-rank experts for test-time continual model merging," in *Advances in Neural Information Processing Systems (NeurIPS)*, 2025, poster (OpenReview). [Online]. Available: <https://openreview.net/forum?id=8DCyv8x580>
- [6] Z. Qiu, L. Wang, Y. Cao, R. Zhang, B. Su, Y. Xu, F. Meng, L. Xu, Q. Wu, and H. Li, "Null-space filtering for data-free continual model merging: Preserving stability, promoting plasticity," in *International Conference on Learning Representations (ICLR)*, 2026, poster. [Online]. Available: <https://openreview.net/forum?id=HDIf3fYqPP>
- [7] G. Liang, Z. Chen, Z. Chen, S. Ji, and Y. Zhang, "New insights on relieving task-recency bias for online class incremental learning," *IEEE Transactions on Circuits and Systems for Video Technology*, vol. 34, no. 5, pp. 3451–3464, 2024.
- [8] R. Wang, X. Duan, G. Kang, J. Liu, S. Lin, S. Xu, J. Lü, and B. Zhang, "Attriclip: A non-incremental learner for incremental knowledge learning," in *Proceedings of the IEEE/CVF Conference on Computer Vision and Pattern Recognition*, 2023, pp. 3654–3663.
- [9] D.-W. Zhou, K.-W. Li, J. Ning, H.-J. Ye, L. Zhang, and D.-C. Zhan, "External knowledge injection for clip-based class-incremental learning," in *Proceedings of the IEEE/CVF International Conference on Computer Vision (ICCV)*, October 2025, pp. 3314–3325.
- [10] L. Huang, X. Cao, H. Lu, and X. Liu, "Class-incremental learning with clip: Adaptive representation adjustment and parameter fusion," in *Computer Vision – ECCV 2024*, 2024, pp. 214–231. [Online]. Available: <https://dblp.org/rec/conf/eccv/HuangCLL24>
- [11] W. Zhang, P. Janson, R. Aljundi, and M. Elhoseiny, "Overcoming generic knowledge loss with selective parameter update," in *Proceedings of the IEEE/CVF Conference on Computer Vision and Pattern Recognition*, 2024, pp. 24 046–24 056.
- [12] G. Zhang, L. Wang, G. Kang, L. Chen, and Y. Wei, "Slca: Slow learner with classifier alignment for continual learning on a pre-trained model," in *Proceedings of the IEEE/CVF International Conference on Computer Vision*, 2023, pp. 19 148–19 158.
- [13] J. Yu, Y. Zhuge, L. Zhang, P. Hu, D. Wang, H. Lu, and Y. He, "Boosting continual learning of vision-language models via mixture-of-experts adapters," in *Proceedings of the IEEE/CVF Conference on Computer Vision and Pattern Recognition*, 2024, pp. 23 219–23 230.
- [14] C. He, Z. Qiu, F. Meng, L. Xu, Q. Wu, and H. Li, "Desclip: Robust continual learning via general attribute descriptions for vlm-based visual recognition," *IEEE Transactions on Multimedia*, pp. 1–16, 2026.
- [15] L. Yu, H. Han, Z. Tao, H. Yao, and C. Xu, "Language guided concept bottleneck models for interpretable continual learning," in *Proceedings of the IEEE/CVF Conference on Computer Vision and Pattern Recognition*, 2025, pp. 14 976–14 986.
- [16] T. Hu, L. Li, Z.-H. Xie, and D.-W. Zhou, "Hierarchical semantic tree anchoring for clip-based class-incremental learning," *arXiv preprint arXiv:2511.15633*, 2025.
- [17] S. Suzuki, S. Yamaguchi, S. Takeda, T. Yamane, N. Makishima, N. Kawata, M. Ihori, T. Tanaka, S. Orihashi, and R. Masumura, "Difference vector equalization for robust fine-tuning of vision-language models," *arXiv preprint arXiv:2511.09973*, 2025.
- [18] L. Huang, X. Cao, H. Lu, Y. Meng, F. Yang, and X. Liu, "Mind the gap: Preserving and compensating for the modality gap in clip-based continual learning," in *Proceedings of the IEEE/CVF International Conference on Computer Vision (ICCV)*, October 2025, pp. 3777–3786.
- [19] Z. Zheng, M. Ma, K. Wang, Z. Qin, X. Yue, and Y. You, "Preventing zero-shot transfer degradation in continual learning of vision-language models," in *Proceedings of the IEEE/CVF International Conference on Computer Vision*, 2023, pp. 19 125–19 136.
- [20] S. Changpinyo, P. Sharma, N. Ding, and R. Soricut, "Conceptual 12m: Pushing web-scale image-text pre-training to recognize long-tail visual concepts," in *Proceedings of the IEEE/CVF conference on computer vision and pattern recognition*, 2021, pp. 3558–3568.
- [21] J. Deng, W. Dong, R. Socher, L.-J. Li, K. Li, and L. Fei-Fei, "Imagenet: A large-scale hierarchical image database," in *2009 IEEE conference on computer vision and pattern recognition*. Ieee, 2009, pp. 248–255.
- [22] J. Lin, "Divergence measures based on the shannon entropy," *IEEE Transactions on Information Theory*, vol. 37, no. 1, pp. 145–151, 1991.
- [23] L. Yu, H. Zhang, and C. Xu, "Text-guided attention is all you need for zero-shot robustness in vision-language models," in *Advances in Neural Information Processing Systems*, 2024.
- [24] C. Liu, Y. Wang, H. Cao, B. Liu, and D. Jiang, "Evaluating the adversarial robustness of vision-language models via internal feature perturbations," *IEEE Transactions on Circuits and Systems for Video Technology*, vol. 36, no. 3, pp. 3938–3950, 2026.
- [25] C. Chen, Z. Li, Y. Zhang, X. Guo, and W. Zhang, "Attention-guided hierarchical defense for multimodal attacks in vision-language models," in *Proceedings of the IEEE/CVF Conference on Computer Vision and Pattern Recognition Workshops*, 2024, pp. 5209–5218.
- [26] B. Wu, W. Shi, J. Wang, and M. Ye, "Synthetic data is an elegant gift for continual vision-language models," in *Proceedings of the IEEE/CVF Conference on Computer Vision and Pattern Recognition (CVPR)*, June 2025, pp. 2813–2823.
- [27] K. Wang, D. Kim, and M. Betke, "Lora-loop: Closing the synthetic replay cycle for continual vlm learning," in *Proceedings of the IEEE/CVF International Conference on Computer Vision (ICCV) Workshops*, October 2025, pp. 445–454.
- [28] Z. Qiu, Y. Xu, F. Meng, H. Li, L. Xu, and Q. Wu, "Dual-consistency model inversion for non-exemplar class incremental learning," in *2024 IEEE/CVF Conference on Computer Vision and Pattern Recognition (CVPR)*. IEEE Computer Society, 2024, pp. 24 025–24 035.
- [29] V. W. Liang, Y. Zhang, Y. Kwon, S. Yeung, and J. Y. Zou, "Mind the gap: Understanding the modality gap in multi-modal contrastive representation learning," *Advances in Neural Information Processing Systems*, vol. 35, pp. 17 612–17 625, 2022.
- [30] M. Zanella and I. Ben Ayed, "Clip-lora: Low-rank adaptation for clip," in *Proceedings of the IEEE/CVF Conference on Computer Vision and Pattern Recognition Workshops*, 2024.
- [31] K. Zhou, J. Yang, C. C. Loy, and Z. Liu, "Learning to prompt for vision-language models," *International Journal of Computer Vision*, vol. 130, no. 9, pp. 2337–2348, 2022.
- [32] K. Zhou, J. Yang, C. C. Loy, and Z. Liu, "Conditional prompt learning for vision-language models," in *Proceedings of the IEEE/CVF conference on computer vision and pattern recognition*, 2022, pp. 16 816–16 825.
- [33] X. Li, D. Lian, Z. Lu, J. Bai, Z. Chen, and X. Wang, "Graphadapter: Tuning vision-language models with dual knowledge graph," *Advances in Neural Information Processing Systems*, vol. 36, 2024.
- [34] Y. Xin, J. Du, Q. Wang, Z. Lin, and K. Yan, "Vmt-adapter: Parameter-efficient transfer learning for multi-task dense scene understanding," in *Proceedings of the AAAI Conference on Artificial Intelligence*, vol. 38, no. 14, 2024, pp. 16 085–16 093.
- [35] E. J. Hu, Y. Shen, P. Wallis, Z. Allen-Zhu, Y. Li, S. Wang, L. Wang, W. Chen *et al.*, "Lora: Low-rank adaptation of large language models." *ICLR*, vol. 1, no. 2, p. 3, 2022.
- [36] M. Boschini, L. Bonicelli, P. Buzzega, A. Porrello, and S. Calderara, "Class-incremental continual learning into the extended der-verse," *IEEE transactions on pattern analysis and machine intelligence*, vol. 45, no. 5, pp. 5497–5512, 2022.
- [37] S. Dong, X. Gao, Y. He, Z. Zhou, A. C. Kot, and Y. Gong, "Ceat: Continual expansion and absorption transformer for non-exemplar class-incremental learning," *IEEE Transactions on Circuits and Systems for Video Technology*, vol. 35, no. 4, pp. 3146–3159, 2024.
- [38] Z. Li and D. Hoiem, "Learning without forgetting," *IEEE transactions on pattern analysis and machine intelligence*, vol. 40, no. 12, pp. 2935–2947, 2017.
- [39] J. Kirkpatrick, R. Pascanu, N. Rabinowitz, J. Veness, G. Desjardins, A. A. Rusu, K. Milan, J. Quan, T. Ramalho, A. Grabska-Barwinska *et al.*, "Overcoming catastrophic forgetting in neural networks," *Proceedings of the national academy of sciences*, vol. 114, no. 13, pp. 3521–3526, 2017.
- [40] Z. Wang, Z. Zhang, C.-Y. Lee, H. Zhang, R. Sun, X. Ren, G. Su, V. Perot, J. Dy, and T. Pfister, "Learning to prompt for continual learning," in *Proceedings of the IEEE/CVF conference on computer vision and pattern recognition*, 2022, pp. 139–149.
- [41] Z. Wang, Z. Zhang, S. Ebrahimi, R. Sun, H. Zhang, C.-Y. Lee, X. Ren, G. Su, V. Perot, J. Dy *et al.*, "Dualprompt: Complementary prompting for rehearsal-free continual learning," in *European Conference on Computer Vision*. Springer, 2022, pp. 631–648.
- [42] J. S. Smith, L. Karlinsky, V. Gutta, P. Cascante-Bonilla, D. Kim, A. Arbelle, R. Panda, R. Feris, and Z. Kira, "Coda-prompt: Continual decomposed attention-based prompting for rehearsal-free continual learning," in *Proceedings of the IEEE/CVF Conference on Computer Vision and Pattern Recognition*, 2023, pp. 11 909–11 919.
- [43] D.-W. Zhou, H.-L. Sun, H.-J. Ye, and D.-C. Zhan, "Expandable subspace ensemble for pre-trained model-based class-incremental learning," in *Proceedings of the IEEE/CVF Conference on Computer Vision and Pattern Recognition*, 2024, pp. 23 554–23 564.

- [44] Y.-S. Liang and W.-J. Li, "Inflora: Interference-free low-rank adaptation for continual learning," in *Proceedings of the IEEE/CVF Conference on Computer Vision and Pattern Recognition*, 2024, pp. 23 638–23 647.
- [45] Z. Gao, J. Cen, and X. Chang, "Consistent prompting for rehearsal-free continual learning," in *Proceedings of the IEEE/CVF Conference on Computer Vision and Pattern Recognition*, 2024, pp. 28 463–28 473.
- [46] D.-W. Zhou, Z.-W. Cai, H.-J. Ye, D.-C. Zhan, and Z. Liu, "Revisiting class-incremental learning with pre-trained models: Generalizability and adaptivity are all you need," *International Journal of Computer Vision*, vol. 133, no. 3, pp. 1012–1032, 2025.
- [47] T. Konishi, M. Kurokawa, C. Ono, Z. Ke, G. Kim, and B. Liu, "Parameter-level soft-masking for continual learning," in *International Conference on Machine Learning*. PMLR, 2023, pp. 17 492–17 505.
- [48] Z. Wang, Z. Zhan, Y. Gong, G. Yuan, W. Niu, T. Jian, B. Ren, S. Ioannidis, Y. Wang, and J. Dy, "Sparcl: Sparse continual learning on the edge," *Advances in Neural Information Processing Systems*, vol. 35, pp. 20 366–20 380, 2022.
- [49] L. Yu, Z. Tao, D. Goswami, H. Yao, B. Twardowski, J. Van de Weijer, C. Xu *et al.*, "Exploiting the semantic knowledge of pre-trained text-encoders for continual learning," *arXiv preprint arXiv:2408.01076*, 2024.
- [50] Y.-C. Yu, C.-P. Huang, J.-J. Chen, K.-P. Chang, Y.-H. Lai, F.-E. Yang, and Y.-C. F. Wang, "Select and distill: Selective dual-teacher knowledge transfer for continual learning on vision-language models," in *Computer Vision – ECCV 2024*, 2024, pp. 219–236. [Online]. Available: <https://dblp.org/rec/conf/eccv/YuHCCLYW24>
- [51] M. Zheng, Y. Tang, Z. Hao, K. Han, Y. Wang, and C. Xu, "Adapt without forgetting: Distill proximity from dual teachers in vision-language models," in *Computer Vision – ECCV 2024*, 2024, pp. 109–125. [Online]. Available: <https://dblp.org/rec/conf/eccv/ZhengTHHWX24>
- [52] I. J. Goodfellow, J. Shlens, and C. Szegedy, "Explaining and harnessing adversarial examples," in *International Conference on Learning Representations (ICLR)*, 2015, poster.
- [53] A. Kurakin, I. J. Goodfellow, and S. Bengio, "Adversarial examples in the physical world," in *Artificial intelligence safety and security*. Chapman and Hall/CRC, 2018, pp. 99–112.
- [54] A. Madry, A. Makelov, L. Schmidt, D. Tsipras, and A. Vladu, "Towards deep learning models resistant to adversarial attacks," in *International Conference on Learning Representations (ICLR)*, 2018, poster. [Online]. Available: <https://openreview.net/forum?id=rJzIBfZAb>
- [55] L. Li, T. Hu, D.-W. Zhou, H.-J. Ye, and D.-C. Zhan, "Bofa: Bridge-layer orthogonal low-rank fusion for clip-based class-incremental learning," *arXiv preprint arXiv:2511.11421*, 2025.
- [56] S. Kullback and R. A. Leibler, "On information and sufficiency," *The annals of mathematical statistics*, vol. 22, no. 1, pp. 79–86, 1951.
- [57] B. Kang, L. Wang, Z. Wu, T. Feng, Y. Li, Y. Gao, and W. Li, "Dynamic multi-layer null space projection for vision-language continual learning," in *Proceedings of the IEEE/CVF International Conference on Computer Vision*, 2025, pp. 2077–2086.
- [58] A. Gomez-Villa, D. Goswami, K. Wang, A. D. Bagdanov, B. Twardowski, and J. van de Weijer, "Exemplar-free continual representation learning via learnable drift compensation," in *European Conference on Computer Vision*. Springer, 2024, pp. 473–490.
- [59] D. Goswami, A. Soutif-Cormerais, Y. Liu, S. Kamath, B. Twardowski, J. Van De Weijer *et al.*, "Resurrecting old classes with new data for exemplar-free continual learning," in *Proceedings of the IEEE/CVF Conference on Computer Vision and Pattern Recognition*, 2024, pp. 28 525–28 534.
- [60] V. Thengane, S. Khan, M. Hayat, and F. Khan, "Clip model is an efficient continual learner," *arXiv preprint arXiv:2210.03114*, 2022.
- [61] S. Jha, D. Gong, and L. Yao, "Clap4clip: Continual learning with probabilistic finetuning for vision-language models," in *Advances in Neural Information Processing Systems*, 2024.
- [62] A. Krizhevsky, G. Hinton *et al.*, "Learning multiple layers of features from tiny images," *Toronto, ON, Canada*, 2009.
- [63] C. Wah, S. Branson, P. Welinder, P. Perona, and S. Belongie, "The caltech-ucsd birds-200-2011 dataset," *California Institute of Technology*, 2011.
- [64] D. Hendrycks, K. Zhao, S. Basart, J. Steinhardt, and D. Song, "The many faces of robustness: A critical analysis of out-of-distribution generalization," in *ICCV*, 2021.
- [65] K. Soomro, A. R. Zamir, and M. Shah, "Ucf101: A dataset of 101 human actions classes from videos in the wild," Center for Research in Computer Vision, University of Central Florida, Tech. Rep. CRCV-TR-12-01, 2012. [Online]. Available: https://www.crcv.ucf.edu/papers/UCF101_CRCV-TR-12-01.pdf
- [66] L. Bottou, "Large-scale machine learning with stochastic gradient descent," in *Proceedings of the 19th International Conference on Computational Statistics (COMPSTAT)*. Springer, 2010, pp. 177–186.
- [67] R. Rombach, A. Blattmann, D. Lorenz, P. Esser, and B. Ommer, "High-resolution image synthesis with latent diffusion models," in *Proceedings of the IEEE/CVF conference on computer vision and pattern recognition*, 2022, pp. 10 684–10 695.
- [68] L. Bossard, M. Guillaumin, and L. Van Gool, "Food-101—mining discriminative components with random forests," in *European conference on computer vision*. Springer, 2014, pp. 446–461.
- [69] O. M. Parkhi, A. Vedaldi, A. Zisserman, and C. Jawahar, "Cats and dogs," in *2012 IEEE conference on computer vision and pattern recognition*. IEEE, 2012, pp. 3498–3505.
- [70] Y. Xu, Y. Chen, J. Nie, Y. Wang, H. Zhuang, and M. Okumura, "Advancing cross-domain discriminability in continual learning of vision-language models," *Advances in Neural Information Processing Systems*, vol. 37, pp. 51 552–51 576, 2024.



Chiyuan He received his M.S. degree in Information and Communication Engineering at the University of Electronic Science and Technology of China (UESTC). He is currently pursuing the Ph.D. degree in UESTC. His main research interests include lifelong learning and multimodal intelligence.



Zihuan Qiu is currently pursuing the Ph.D. degree in University of Electronic Science and Technology of China, Chengdu, China. His current research interests include continual learning and machine learning.



Fanman Meng (Member, IEEE) received the Ph.D. degree in Signal and Information Processing from the University of Electronic Science and Technology of China, Chengdu, China, in 2014. From 2013 to 2014, he was a Research Assistant with the Division of Visual and Interactive Computing, Nanyang Technological University, Singapore. He is currently a Professor with the School of Information and Communication Engineering, University of Electronic Science and Technology of China. He has authored or co-authored numerous technical articles in well-known international journals and conferences. His current research interests include image segmentation and object detection.



Runtong Zhang is currently working toward the Ph.D. degree with the School of Information and Communication Engineering, University of Electronic Science and Technology of China, Chengdu, 611731, China. His current research interests include semantic segmentation, domain generalization, few/zero-shot learning.



Hongliang Li (Senior Member, IEEE) received his Ph.D. degree in Electronics and Information Engineering from Xi'an Jiaotong University, China, in 2005. From 2005 to 2006, he joined the visual signal processing and communication laboratory (VSPC) of the Chinese University of Hong Kong (CUHK) as a Research Associate. From 2006 to 2008, he was a Postdoctoral Fellow at the same laboratory in CUHK. He is currently a Professor in the School of Information and Communication Engineering, University of Electronic Science and Technology of China. His research interests include image segmentation, object detection, image and video coding, visual attention, and multimedia processing.

Dr. Li has authored or co-authored numerous technical articles in well-known international journals and conferences. He is a co-editor of a Springer book titled "Video segmentation and its applications". Dr. Li is involved in many professional activities. He received the 2019 and 2020 Best Associate Editor Awards for IEEE Transactions on Circuits and Systems for Video Technology (TCSVT), and the 2021 Best Editor Award for Journal on Visual Communication and Image Representation. He served as a Technical Program Chair for VCIP 2016 and PCM 2017, General Chairs for ISPACS 2017 and ISPACS 2010, a Publicity Chair for IEEE VCIP 2013, a Local Chair for the IEEE ICME 2014, Area Chairs for VCIP 2022 and 2021, and a Reviewer committee member for IEEE ISCAS from 2018 to 2022. He served as an Associate Editor of IEEE Transactions on Circuits and Systems for Video Technology (2018-2021). He is now an Associate Editor of Journal on Visual Communication and Image Representation, IEEE Open Journal of Circuits and Systems, and an Area Editor of Signal Processing: Image Communication (Elsevier Science). He is selected as the IEEE Circuits and Systems Society Distinguished Lecturer for 2022-2023.



Linfeng Xu (Member, IEEE) received the Ph.D. degree in Signal and Information Processing from the School of Electronic Engineering, University of Electronic Science and Technology of China (UESTC), Chengdu, China, in 2014. From December 2014 to December 2015, he was with the Ubiquitous Multimedia Laboratory, the State University of New York at Buffalo, USA, as a visiting scholar. He is currently an Associate Professor with the School of Information and Communication Engineering, UESTC. His research interests include machine learning, computer vision, visual signal processing, artificial intelligence theory and applications. He served as a Local Arrangement Chair for ISPACS 2010 and VCIP 2016.

He is currently an Associate Professor with the School of Information and Communication Engineering, UESTC. His research interests include machine learning, computer vision, visual signal processing, artificial intelligence theory and applications. He served as a Local Arrangement Chair for ISPACS 2010 and VCIP 2016.



Qingbo Wu (Member, IEEE) received the Ph.D. degree in signal and information processing from the University of Electronic Science and Technology of China in 2015. From February 2014 to May 2014, he was a Research Assistant with the Image and Video Processing (IVP) Laboratory, Chinese University of Hong Kong. From October 2014 to October 2015, he served as a Visiting Scholar with the Image and Vision Computing (IVC) Laboratory, University of Waterloo. He is currently a Professor with the School of Information and Communication

Engineering, University of Electronic Science and Technology of China. His research interests include image/video coding, quality evaluation, perceptual modeling and processing. He has served as Area Chair for ACM MM 2024-2025, VCIP 2016, Session Chair for ACM MM 2021, ICMCT 2022, TPC/PC member of AAAI 2021-2023, APSIPA ASC 2020-2021, CICA 2021-2023. He was also a Guest Editor of Remote Sensing and Frontiers in Neuroscience.